

Diatomic molecule as a testbed for combining DMFT with electronic structure methods such as GW and DFT

Juho Lee and Kristjan Haule

Department of Physics & Astronomy, Rutgers University, Piscataway, NJ 08854-8019, USA

(Dated: November 17, 2021)

We implemented combination of DMFT and GW in its fully self-consistent way, one shot GW approximation, and quasiparticle self-consistent scheme, and studied how well these combined methods perform on H_2 molecule as compared to more established methods such as LDA+DMFT. We found that most flavors of GW +DMFT break down in strongly correlated regime due to causality violation. Among GW +DMFT methods, only the self-consistent quasiparticle GW +DMFT with static double-counting, and a new method with causal double-counting, correctly recover the atomic limit at large H-atom separation. While some flavors of GW +DMFT improve the single-electron spectra as compared to LDA+DMFT, the total energy is best predicted by LDA+DMFT, for which the exact double-counting is known, and is static.

I. INTRODUCTION

In last couple of decades, many theories have been developed to tackle the problem of strong correlations in systems where conventional methods based on the density functional theory (DFT) [1, 2] encounter difficulties. Kinetic energy and electronic interaction are comparable in those materials, and electrons display a mixed behavior between particles and waves. This makes the problem complicated even for low-energy lattice models with limited number of degrees of freedom. Such delocalization-localization interplay of electron is the key to the numerous interesting phenomena in condensed matter physics including tunable magnetism, colossal magnetoresistance, heavy fermion behavior, high-Tc superconductivity and metal insulator transition.

Among many theoretical developments, the dynamical mean-field theory (DMFT) [3, 4] has been very successful, and due to its non-perturbative nature it was able to describe the phenomena of the first order metal insulator transition even in its most simplistic form of the single band Hubbard model. [4] Due to the flexibility of the DMFT, it has been extended in many directions, adding bosonic bath to treat long range spin [5, 6] or coulomb interactions [7], extending the range of correlations from a site to clusters [8] to address the issue of momentum space differentiation, and finally it has been combined with DFT to become more realistic [9]. This combination of DFT and DMFT (DFT+DMFT) has been very successful in describing materials with open d and f shells both for their spectral properties, as well as computing total energy [10] and free energy [11] of crystal phases. Recently, DMFT has also been successfully applied to molecules [12, 13].

Hedin's GW approximation [14, 15] is a many-body perturbative technique, which approximates the self-energy by the lowest order diagram in the screened Coulomb interaction: $\Sigma = -GW$. As opposed to the ground state nature of DFT, where the gaps of the Kohn-Sham spectrum have no physical meaning, in GW approximation the target is the single particle Green's func-

tion and therefore the single particle excitation spectrum of GW is expected to be a better prediction than the Kohn-Sham spectrum. Since GW is a diagrammatic method and DMFT can also be expressed in the diagrammatic form, the combination of the GW and DMFT (GW +DMFT) was proposed [16, 17] as a possibly better alternative to DFT+DMFT. Furthermore, the momentum dependence of GW self-energy is expected to complement the local nature of the DMFT, in particular when the DMFT locality is enforced in less localized basis, such as in the basis of Wannier orbitals. [18–20].

Most of GW calculations for solid-state systems in practice rely on one-shot GW scheme (generally denoted as G_0W_0). In this scheme, the GW self-energy is computed only once and the non-interacting Green's function G_0 is obtained from the Kohn-Sham DFT spectrum [21]. The one-shot GW method has been successful for many materials with weak to moderate electronic correlation, giving a very good approximation for bandgaps in semiconductors [22]. To remove the dependence on the DFT spectrum through G_0 , the scheme called quasiparticle self-consistent QS- GW was developed [23–25] where the non-interacting G_0 is determined in a self-consistent way from the GW spectrum.

While the success of the DFT+DMFT is now supported by the numerous applications to solid state systems, which are too many to review here, the GW +DMFT method is still in its infancy. Nevertheless, several calculations implementing some flavor of GW +DMFT have been reported recently, both for real materials [26–30] and for models [31–33]. However a comprehensive test of numerous GW +DMFT schemes, and their appropriateness for calculating spectra or energy, is still lacking.

Small molecules have served as very good test beds to investigate electronic structure methods. For example, Lin *et al.* [12] applied DMFT to hydrogen chain (H_n) where they found the cluster DMFT produces comparable accuracy to density matrix renormalization group (DMRG). Our previous study of LDA+DMFT on H_2 molecule [34] demonstrated that single-site DMFT with a good choice of local orbitals and exact double-counting

method gives extremely precise total energy, and also considerably improves the spectra, as compared to LDA.

Here we perform a comprehensive test of various flavors of GW+DMFT, from fully self-consistent GW +DMFT to G_0W_0 +DMFT and QSGW+DMFT. We compute the total energy and the spectra of H_2 molecule for all these methods, and compare them to DFT+DMFT and the exact solution.

We find that the strongly correlated regime is very challenging for most of GW+DMFT methods, and most of them fail due to causality violation, which has not been properly addressed before. The only exception proposed before is the quasiparticle self-consistent method, i.e., QSGW+DMFT. The latter recovers the correct atomic limit only when combined with the static double-counting, in which case it gives comparable spectra and energy to the results of LDA+DMFT. We propose here a new causal double-counting scheme, which works better than other GW+DMFT schemes in the strongly correlated regime.

Close to the equilibrium volume, which can be characterized as the weakly to moderately correlated regime, most of GW+DMFT schemes considerably improve the spectra, as compared to LDA+DMFT. However, the total energy of GW+DMFT rivals LDA+DMFT total energy only in the fully self-consistent version, which however breaks down in the correlated regime. The quasiparticle method with static double-counting, which performs well in the correlated regime, does not give very accurate total energy in the moderately correlated regime, as it is not derivable from a functional.

Our study demonstrates that the QSGW+DMFT, in combination with static double-counting, is a promising direction for computing spectra of correlated systems both in moderate to strongly correlated regime. On the other hand, the GW+DMFT methods tested in this work, do not rival LDA+DMFT in predicting the total energy of the system.

II. METHODS

A. Approximations derived from a Functional: DMFT, LDA+DMFT, and GW+DMFT

Let us start by refreshing the Baym-Kadanoff (BK) formalism [35, 36], which provides the functional of the Green's function G

$$\Gamma[G] = \text{Tr} \log G - \text{Tr}((G_0^{-1} - G^{-1})G) + \Phi_v[G], \quad (1)$$

that is stationary for the exact Green's function G , and gives the grand potential, when evaluated on the exact Green's function G (for details see also [9]). Here G_0 is the non-interacting Green's function $G_0^{-1} = [i\omega + \mu - \nabla^2 + V_{ext}(\mathbf{r})]\delta(\mathbf{r}, \mathbf{r}')$ and V_{ext} is the potential due to nuclei. The last term $\Phi_v[G]$ is the so-called Luttinger-Ward (LW) functional, which is the sum of all skeleton diagrams constructed by the Green's function G and the

Coulomb repulsion $v(\mathbf{r}, \mathbf{r}') = \frac{1}{|\mathbf{r}-\mathbf{r}'|}$. The derivative of the LW functional with respect to G gives the exact self-energy of the system

$$\frac{\delta\Phi_v[G]}{\delta G} = \Sigma. \quad (2)$$

The stationarity of the functional $\Gamma[G]$ at the exact G ($\delta\Gamma/\delta G = 0$) is ensured by the Dyson equation

$$G^{-1} - [i\omega + \mu - \nabla^2 + V_{ext}(\mathbf{r})]\delta(\mathbf{r}, \mathbf{r}') + \Sigma = 0. \quad (3)$$

The functional $\Phi_v[G]$ is diagrammatically known, but its evaluation is extremely difficult due to fermionic minus sign problem [37]. Nevertheless, this formalism is extremely useful because many good approximations can be devised by approximating Φ rather than Γ , and such approximations were shown to be conserving [35, 36].

One can classify these approximations into two classes: those that truncate correlations in the real space, and those that truncate in the space of Feynman diagrams. In LDA the functional Φ is truncated in real space so that exchange and correlations are local to a point in 3D space, i.e., each point in 3D space is mapped to an independent auxiliary problem of electron gas. In the DMFT the functional Φ is also truncated in real space, but the locality is constraint to a site on the lattice, which is mapped to an auxiliary problem of quantum impurity.

On the other hand, in Hartree-Fock and GW theories, the truncation is done in the space of Feynman diagrams but the complete space dependence of the self-energy is kept. The GW +DMFT can then be seen as the hybrid between these two classes of approaches, as it truncates Feynman diagrams only for the long range part of the correlations, while the short-range correlations can be exactly accounted for by the DMFT.

1. DMFT

In the DMFT method, the locality of correlations is explored and the LW-functional is truncated so that it is a functional of the local Green's function (G_{loc}) only, i.e., it contains all skeleton Feynman diagrams that are constructed from G_{loc} and interaction v , and all diagrams that are outside this range, are neglected. In real material calculation, the DMFT method is defined only, once the projector to the local Green's function is specified. In this work, we will use the real space projectors, defined by

$$G_{loc}^{\mathbf{R}} = \hat{P}G \equiv \sum_{LL'} |\chi_{\mathbf{R}}^L\rangle \langle \chi_{\mathbf{R}}^L | G | \chi_{\mathbf{R}}^{L'}\rangle \langle \chi_{\mathbf{R}}^{L'}|. \quad (4)$$

where $\{|\chi_{\mathbf{R}}^L\rangle\}$ is a local orbital set centered on a given nucleus at \mathbf{R} , and L is an orbital index. In the single-orbital DMFT case, which we will test in this work, no sum over L is needed.

The DMFT LW-functional is then

$$\Phi^{\text{DMFT}}[G] = \sum_{\mathbf{R}} \Phi_v[G_{loc}^{\mathbf{R}}]. \quad (5)$$

and the functional $\Phi_v[G_{loc}]$ has the same dependence on G_{loc} as the exact functional $\Phi_v[G]$ on G , except that it has finite range. This is because any Feynman diagram of arbitrary topology that is contained in exact $\Phi_v[G]$ is also contained in approximate $\Phi_v[G_{loc}]$. In solid state applications of DMFT, the interaction v has to be replaced by the screened interaction \mathcal{U} due to the fact that many degrees of freedom are being removed from consideration. Screening in molecules is negligible, hence we can safely take $\mathcal{U} = v$ for the molecular systems.

To compute $\Phi_v[G_{loc}^{\mathbf{R}}]$ the system is mapped to a quantum impurity model, for which $\mathcal{G}_{imp} = G_{loc}^{\mathbf{R}}$ so that the exact solution of the impurity problem $\Phi_v[\mathcal{G}_{imp}]$ delivers the desired LW functional. The DMFT self-energy is then obtained from the auxiliary impurity self-energy, as required by the Baym-Kadanoff formalism:

$$\begin{aligned} \Sigma^{\text{DMFT}} &= \frac{\delta \Phi^{\text{DMFT}}}{\delta G} = \sum_{\mathbf{R}} \frac{\delta G_{loc}^{\mathbf{R}}}{\delta G} \frac{\delta \Phi_v[G_{loc}^{\mathbf{R}}]}{\delta G_{loc}^{\mathbf{R}}} \\ &= \sum_{\mathbf{R}, LL'} |\chi_{\mathbf{R}}^L\rangle \Sigma_{imp}^{\mathbf{R}, LL'} \langle \chi_{\mathbf{R}}^{L'} | \equiv \hat{E} \Sigma_{imp} \end{aligned} \quad (6)$$

where we define the embedding \hat{E} . This embedding process is the inverse operation of the projector \hat{P} , mapping the self-energy of the auxiliary impurity back into the Hilbert space of the original system.

2. LDA+DMFT

In the LDA+DMFT formalism, the LW functional is approximated by the combination of LDA and DMFT functional

$$\begin{aligned} \Phi^{\text{LDA+DMFT}}[G] &= E_v^H[\rho] + E_v^X[\rho] + E_v^{\text{LDA},C}[\rho] \\ &+ \sum_{\mathbf{R}} (\Phi_v[G_{loc}^{\mathbf{R}}] - \Phi^{DC}[G_{loc}^{\mathbf{R}}]) \end{aligned} \quad (7)$$

where the double-counting (DC) correction Φ^{DC} subtracts the intersection of the two approximations. The Hartree, exchange, and correlation functional of the LDA are

$$E_v^H[\rho] = \frac{1}{2} \int_{\mathbf{r}\mathbf{r}'} \rho(\mathbf{r})v(\mathbf{r}-\mathbf{r}')\rho(\mathbf{r}') \quad (8)$$

$$E_v^X[\rho] = -\frac{1}{2} \sum_{\sigma} \int_{\mathbf{r}\mathbf{r}'} \rho^{\sigma}(\mathbf{r},\mathbf{r}')v(\mathbf{r}-\mathbf{r}')\rho^{\sigma}(\mathbf{r}',\mathbf{r}) \quad (9)$$

$$E_v^{\text{LDA},C}[\rho] = \int_{\mathbf{r}} \rho(\mathbf{r})\varepsilon_v^{\text{LDA},C}[\rho(\mathbf{r})]. \quad (10)$$

We used the Vosko-Wilk-Nusair (VWN) parametrization for the LDA correlation energy [38].

When applying the DMFT approximation on the LDA functional, (or, applying the LDA approximation on the DMFT functional) we get the following expression for the "exact" double-counting:

$$\Phi^{DC}[G_{loc}^{\mathbf{R}}] = E_v^H[\rho_{loc}^{\mathbf{R}}] + E_v^X[\rho_{loc}^{\mathbf{R}}] + E_v^{\text{LDA},C}[\rho_{loc}^{\mathbf{R}}] \quad (11)$$

where $\rho_{loc}^{\mathbf{R}}$ is the projected local density $\rho_{loc}^{\mathbf{R}} = G_{loc}^{\mathbf{R}}(\tau = 0^-)$ at the site \mathbf{R} . As shown in Ref. [34], this LDA+DMFT with the exact double-counting leads to very accurate results in H_2 molecule. Note that such exact double-counting can also be extended to solid state systems, but in this case one needs to replace Coulomb interaction v with the screened interaction \mathcal{U} in the functional Eq. 11. [39]

3. GW+DMFT

The GW self-energy is the first order approximation of screened interaction $\Sigma^{GW} = -GW$ (we follow here the sign convention of the imaginary time formalism). The screened interaction $W = v/(1 - Pv)$ is approximated by the RPA polarization $P = 2GG$ where the factor 2 is for spin degrees of freedom. From (2), its functional form can be written as

$$\Phi_v^{GW}[G] = - \sum_{n=1}^{\infty} \frac{1}{2n} \text{Tr}[(2GvG)^n] = \frac{1}{2} \text{Tr} \log(1 - 2GvG) \quad (12)$$

where the first term (n=1) corresponds to the exchange functional $E_v^X[\rho]$.

Just like in LDA+DMFT, LW functional of GW +DMFT is a combination of GW functional augmented with the DMFT functional for the local degrees of freedom, i.e.,

$$\begin{aligned} \Phi^{GW+DMFT}[G] &= E_v^H[\rho] + \Phi_v^{GW}[G] \\ &+ \sum_{\mathbf{R}} (\Phi_v[G_{loc}^{\mathbf{R}}] - \Phi^{DC}[G_{loc}^{\mathbf{R}}]). \end{aligned} \quad (13)$$

The double-counting of GW +DMFT is obtained by applying the DMFT approximation on the GW functional, leading to

$$\begin{aligned} \Phi^{DC}[G_{loc}^{\mathbf{R}}] &= E_v^H[\rho_{loc}^{\mathbf{R}}] + \Phi_v^{GW}[G_{loc}^{\mathbf{R}}] \\ &= E_v^H[\rho_{loc}^{\mathbf{R}}] + \frac{1}{2} \text{Tr} \log(1 - 2G_{loc}^{\mathbf{R}}vG_{loc}^{\mathbf{R}}). \end{aligned} \quad (14)$$

To converge the GW +DMFT equations, we implemented the following steps:

- (1) Starting with an initial non-interacting Green's function $G = G_0$, we construct

$$P(\tau) = 2G(\tau)G(-\tau) \quad (15)$$

$$W(i\nu) = v/(1 - P(i\nu)v) \quad (16)$$

where all variables above are general matrices.

(2) The GW self-energy is given by:

$$\Sigma^{GW}(\mathbf{r}\mathbf{r}'; \tau) = -G(\mathbf{r}\mathbf{r}'; \tau)W(\mathbf{r}\mathbf{r}'; \tau) \quad (17)$$

(3) From (14), we see that the double-counted GW contribution to the self-energy is :

$$\Sigma_{DC}^{GW}(\tau) = \frac{\delta\Phi_v^{GW}[G_{loc}^{\mathbf{R}}]}{\delta G_{loc}^{\mathbf{R}}} = -G_{loc}^{\mathbf{R}}(\tau)W_{loc}(\tau) \quad (18)$$

where the local components are computed by

$$G_{loc}^{\mathbf{R}} = \hat{P}^{\mathbf{R}}G \quad (19)$$

$$P_{loc}(\tau) = 2G_{loc}^{\mathbf{R}}(\tau)G_{loc}^{\mathbf{R}}(-\tau) \quad (20)$$

$$W_{loc}(i\nu) = v/(1 - P_{loc}(i\nu)v). \quad (21)$$

(4) Electron density is given by $\rho = G(\tau = 0^-)$.

(5) Next we calculate the Hartree potential

$$V^H(\mathbf{r}) = \frac{\delta\Phi^H[\rho]}{\delta\rho(\mathbf{r})} = \int d\mathbf{r}'v(\mathbf{r} - \mathbf{r}')\rho(\mathbf{r}'). \quad (22)$$

(6) (*DMFT loop*) Using local Green's function at each site $G_{loc}^{\mathbf{R}} = \hat{P}^{\mathbf{R}}G$ and the interaction v , we construct the auxiliary impurity model, which delivers the impurity self-energy

$$\Sigma_{imp} = \frac{\delta\Phi_v[G_{loc}^{\mathbf{R}}]}{\delta G_{loc}^{\mathbf{R}}} \quad (23)$$

(7) Putting together GW , $DMFT$ and DC , the total self-energy is obtained by

$$\Sigma = \Sigma^{GW} + \sum_{\mathbf{R}, LL'} |\chi_{\mathbf{R}}^L\rangle (\Sigma_{imp}^{\mathbf{R}, LL'} - \Sigma_{DC}^{\mathbf{R}, LL'}) \langle \chi_{\mathbf{R}}^{L'} | \quad (24)$$

The double-counting is $\Sigma_{DC}(i\omega) = V_{loc}^H + \Sigma_{DC}^{GW}(i\omega)$, with Σ_{DC}^{GW} evaluated in (3), and the local Hartree V_{loc}^H is

$$\begin{aligned} V_{loc}^H &= \frac{\delta\Phi^H[\rho_{loc}]}{\delta\rho_{loc}} \\ &= \sum_{LL'} |\chi_{\mathbf{R}}^L\rangle \langle \chi_{\mathbf{R}}^L | V^H[\rho_{loc}] | \chi_{\mathbf{R}}^{L'}\rangle \langle \chi_{\mathbf{R}}^{L'}|. \end{aligned} \quad (25)$$

(8) From Dyson equation (3), the total Green's function is given by

$$G^{-1} = [i\omega + \mu + \nabla^2 - V_{ext} - V^H]\delta(\mathbf{r} - \mathbf{r}') - \Sigma(\mathbf{r}\mathbf{r}'; i\omega), \quad (26)$$

where the chemical potential is determined by enforcing charge neutrality, i.e.,

$$\int d\mathbf{r}\rho(\mathbf{r}) = \int d\mathbf{r}G(\mathbf{r}, \mathbf{r}; \tau = 0^-) = Z_{nuclei} \quad (27)$$

(9) For *Fully self-consistent GW+DMFT*, go back to (1). All variables are updated until self-consistency is reached. For G_0W_0+DMFT , go to (4). Therefore the GW self-energy (17) and its local counterpart (18) do not change over the iterative process while the impurity self-energy, total density and the Green's function are updated.

B. Quasiparticle self-consistent $GW+DMFT$ and its double-counting

First, let us discuss the quasiparticle self-consistent GW [23–25]. It is similar to G_0W_0 in that the polarization $P = 2G^{QP}G^{QP}$ and the self-energy $\Sigma = -G^{QP}W^{QP}$ are computed from a free-particle Green's function $G^{QP} = 1/(\omega + \mu - H^{QP})$, in which H^{QP} is a Hermitian non-interacting Hamiltonian, which is however determined in a self-consistent way from the GW spectra.

Refs. [23–25] proposed to solve the following quasiparticle equation

$$[-\nabla^2 + V_{ext} + V^H + \text{Re}\Sigma^{GW}(E_n) - E_n]|\psi_n\rangle = 0. \quad (28)$$

to determine the Hermitian quasiparticle Hamiltonian with the form $[H^{QP} - E_n]|\psi_n\rangle = 0$.

Since the GW self-energy has a weak frequency dependence, we may use $\text{Re}\Sigma^{GW}(\omega) \approx \text{Re}\Sigma^{GW}(0) + \frac{\partial\text{Re}\Sigma^{GW}(0)}{\partial\omega}\omega = \text{Re}\Sigma^{GW}(0) + (1 - Z^{-1})\omega$ where the quasiparticle renormalization amplitude matrix is

$$Z^{-1} = \mathbb{1} - \frac{\partial\text{Re}\Sigma^{GW}(0)}{\partial\omega}, \quad (29)$$

which gives the following form for the quasiparticle Hamiltonian

$$H^{QP} = Z^{1/2}[-\nabla^2 + V_{ext} + V^H + \text{Re}\Sigma^{GW}(0)]Z^{1/2}. \quad (30)$$

Since the $QSGW$ procedure provides a static effective Hamiltonian in which the GW spectral information is encoded, one might think that $QSGW$ Hamiltonian can simply replace the KS Hamiltonian of $DFT+DMFT$ and yield better accuracy. However, to implement $QSGW+DMFT$, there is a subtle issue concerning the double-counting between the H^{QP} and $DMFT$ correlation.

Since H^{QP} is constructed based on the real part of GW self-energy, one may attempt to approximate $H^{QP} + \Sigma(i\omega) = H^{QP} + \hat{E}(\Sigma_{imp}(i\omega) - \text{Re}\Sigma_{DC}^{GW}(i\omega))$. But this self-energy obviously violates the causality condition as it does not respect the Kramers-Kronig relation. In the following, we will introduce two double-counting schemes, which obey the Kramers-Kronig relation.

1. Static double-counting (SDC)

In the simplest approach, we can take the double-counting as the zero-frequency value of the local- GW self-energy, i.e.,

$$\Sigma^{SDC} = V_{loc}^H + \text{Re}\Sigma_{DC}^{GW}(\omega = 0) \quad (31)$$

where Σ_{DC}^{GW} is the exact DC given by Eq. (18). Recently, the combined method $QSGW+DMFT$, has been implemented for real materials in Ref. [30], in which the static double-counting was employed.

We implement $QSGW+DMFT$ as follows:

- (1) We start with initial values for G^{QP} , $\rho(\mathbf{r})$ and $\Sigma_{\text{imp}}(i\omega)$. We take their LDA counterparts H^{KS} , $(G^{\text{QP}})^{-1} = i\omega + \mu - H^{KS}$ and ρ^{LDA} . For the impurity self-energy, we start with the local Hartree-Fock.
- (2) Self-energies are constructed $\Sigma^{GW} = -G^{\text{QP}}W^{\text{QP}}$ and $\Sigma_{DC}^{GW} = -G_{\text{log}}^{\text{QP}}W_{\text{loc}}^{\text{QP}}$ and then we obtain the double counting $\Sigma^{SDC} = V_{\text{loc}}^H + \Sigma_{DC}^{GW}(w=0)$.
- (3) Next, the Hartree potential is computed from the density

$$V^H(\mathbf{r}) = \frac{\delta\Phi^H[\rho]}{\delta\rho(\mathbf{r})} = \int d\mathbf{r}' v(\mathbf{r} - \mathbf{r}')\rho(\mathbf{r}'). \quad (32)$$

- (4) The quasiparticle Hamiltonian H^{QP} is computed using Eq. (30), so that new $(G^{\text{QP}})^{-1} = i\omega + \mu - H^{\text{QP}}$.
- (5) The total Green's function is then given by

$$G = \frac{1}{i\omega + \mu - H^{\text{QP}} - \hat{E}(\Sigma_{\text{imp}} - \Sigma^{SDC})}. \quad (33)$$

- (6) The density and the chemical potential are computed from $\rho(\mathbf{r}) = G(\mathbf{r}, \mathbf{r}, \tau = 0^{-1})$.
- (7) (DMFT loop) from the local Green's function $G_{\text{loc}}^{\mathbf{R}} = \hat{P}^{\mathbf{R}}G$ and the interaction v , the impurity solver calculates a new impurity self-energy:

$$(G_{\text{loc}}^{\mathbf{R}}, v) \rightarrow \Sigma_{\text{imp}}(i\omega). \quad (34)$$

- (8) With updated variables G^{QP} , ρ and Σ^{imp} , go to the step (2).

The main difference between our QSGW+DMFT and that of Ref. [30] is that the quasiparticle H^{QP} in Ref. [30] was calculated from QSGW only, and the feedback of the DMFT self-energy on H^{QP} was ignored. In our case, we recompute H^{QP} from the physical self-consistent Green's function in every iteration.

2. Dynamical double-counting (DDC)

Although the static local GW term is subtracted, one can expect that the spectral function is possibly over-renormalized because H^{QSGW} , which is renormalized by GW , is again renormalized by the DMFT self-energy.

This is a very subtle issue for QSGW+DMFT because the dynamical effects of GW self-energy are incorporated in the static QSGW Hamiltonian H^{QP} , therefore we would like to subtract the local part of this renormalization.

To overcome this problem, we first construct a *non-local* quasiparticle Hamiltonian $H_{\text{nonloc}}^{\text{QP}}$ where not only

GW but also the subtraction of the local GW is incorporated. The bandwidth of correlated orbitals of $H_{\text{nonloc}}^{\text{QP}}$ must be wider than H^{QP} because we *unrenormalize* the local GW effect in $H_{\text{nonloc}}^{\text{QP}}$. This widened band is then corrected by the impurity self-energy, which is expected to be more accurate than the local GW self-energy.

In order to define the non-local quasiparticle Hamiltonian $H_{\text{nonloc}}^{\text{QP}}$, using the non-local GW self-energy we write

$$\Sigma_{\text{nonloc}}^{GW}(\omega) = \Sigma^{GW}(\omega) - \Sigma_{DC}^{GW}(\omega), \quad (35)$$

and we compute

$$\bar{Z}^{-1} = \mathbb{1} - \frac{\partial \Sigma_{\text{nonloc}}^{GW}(0)}{\partial \omega} \quad (36)$$

and then we define

$$H_{\text{nonloc}}^{\text{QP}} = \bar{Z}^{1/2} [-\nabla + V_{\text{ext}} + V^H + \Sigma_{\text{nonloc}}^{GW}(0)] \bar{Z}^{1/2}. \quad (37)$$

The above algorithm then has to be modified so that the step (5) in computing the total Green's function uses

$$G = \frac{1}{i\omega + \mu - H_{\text{nonloc}}^{\text{QP}} - \hat{E}(\Sigma_{\text{imp}} - V_{\text{loc}}^H)}. \quad (38)$$

rather than (33).

This DDC approach shares the basic idea of the scheme introduced by Tomczak in Ref. [40], where he calculated the $H_{\text{nonloc}}^{\text{QP}}$ along the real frequency. On the other hand, we implement the scheme based on the Matsubara formalism using linearization of the GW self-energy.

C. Causal double-counting scheme for GW +DMFT

We propose here another type of double-counting for GW +DMFT, which we denote as *causal double-counting* (CDC). As will be clear in the III. A. 1, GW +DMFT with the exact double-counting (Eq. (18)) suffers a causality violation that does not allow GW +DMFT to work in the strongly correlated regime. To avoid the causality breakdown, we introduce causal double-counting (CDC) functional

$$\Sigma^{DC} = \hat{P}\Sigma^{GW}. \quad (39)$$

and we will discuss why this double-counting scheme allows us to avoid the causality issue in the III. A. 2.

One can notice that the CDC is not exact because this double-counting contains the diagrams in which the degrees of freedom of the DMFT local orbitals and the rest of the space interact through the screened interaction W , which is not contained in the DMFT self-energy. Nevertheless, it allows GW +DMFT to work in the strongly correlated regime without violating the causality.

D. Computational details

In this work we use only the single site DMFT combined with LDA and various flavors of GW. We use the same choice of the DMFT projector as in our previous study of LDA+DMFT [34], the linear combination of the lowest two orbitals of H_2^+ cation, $|1s\sigma_g\rangle$ (bonding) and $|1p\sigma_u\rangle$ (anti-bonding) state. We denote them as the “left” (L) and the “right” (R) localized orbital:

$$\begin{aligned} |\chi_L\rangle &= \frac{1}{\sqrt{2}}(|1s\sigma_g\rangle - |1p\sigma_u\rangle), \\ |\chi_R\rangle &= \frac{1}{\sqrt{2}}(|1s\sigma_g\rangle + |1p\sigma_u\rangle). \end{aligned} \quad (40)$$

This orbital set is a good choice for the DMFT projector because i) they are well-localized at each atomic site, ii) they naturally recover $1s$ orbital (the ground state of H) on each site at large atomic separation, iii) over 96% of the electronic charge of the DMFT solution is contained in these two states, which implies most of correlation can be captured within the single site approach, and iv) they do not explicitly depend on the self-consistent charge density. The last condition is especially important for a stationarity of the DMFT solution, given that we are extremizing the Luttinger-Ward functional.

Since H_2^+ is a one-electron problem, the solution is achieved by solving the single-particle Schrödinger’s equation. We follow a recursive approach (see Ref. [41]) to solve H_2^+ cation and several lowest orbital energies are presented in Fig. 1.

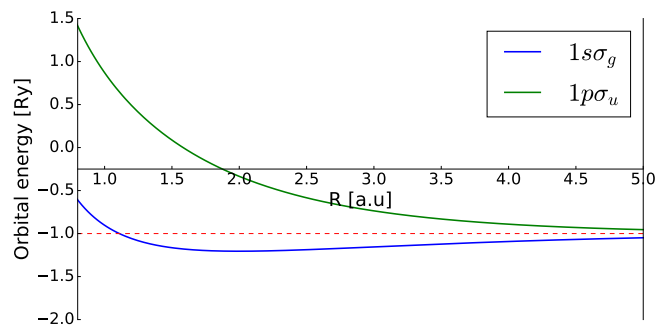


FIG. 1. (Color online) The lowest two orbital energies of H_2^+ cation as a function of R , which are taken to define the DMFT projector (Eq. (40)).

The entire Hilbert space of H_2 is spanned by approximately 30 Gaussian orbitals (correlation-consistent basis set, cc-pVTZ [42]). We want to emphasize that the GW calculation in this study is converged with respect to the size of the basis set, which is very challenging in solid state applications, and this is another reason why such tests of GW +DMFT are important and useful.

We evaluate the ground state energy of GW +DMFT schemes using the Galitskii-Migdal formula

$$E = \text{Tr}(H_0\rho) + \frac{1}{2}\text{Tr}(\Sigma G) \quad (41)$$

where H_0 is the non-interacting part of Hamiltonian $H_0 = -\nabla^2 + v_{ext}$, ρ is the total electron density, and G is the total Green’s function of the system.

The inverse temperature is set to be $\beta = 1/k_B T = 100\text{Ry}^{-1}$. Since the orbital energy gap of H_2 is order of several Ry , this temperature is sufficiently low and therefore describes the ground state.

III. RESULTS AND DISCUSSION

The H_2 molecule is a archetypical correlated system, often taken as an example to demonstrate the failure of methods that use the single slater determinant ansatz, such as Hartree-Fock and LDA. In the dissociation limit, such methods predict delocalized ground state, which never recovers correct atomic limit. GW approximation, a many-body perturbative method, only slightly improves on LDA in this strongly correlated limit as well. The electronic correlations are only moderate around equilibrium distance ($R = 1.4$ a.u.), nevertheless none of these methods (LDA, HF or GW) give an accurate total energy compared to the exact solution, achieved by the configuration interaction (CI) method.

In addition the prediction of the ionization energy (IE) from single particle spectral function is a very good indicator of the quality of the predicted single particle spectra within a given approximation. As is known from the exact solution, the ionization energy is the energy required to remove a single electron, i.e.,

$$\begin{aligned} \text{H}_2 + \text{IE} &\rightarrow \text{H}_2^+ + e^- \\ \Rightarrow \text{IE} &= E(\text{H}_2^+) - E(\text{H}_2) \end{aligned} \quad (42)$$

where $E(\text{H}_2^+)$ is the ground state energy of H_2^+ . We computed the single particle Green’s function in all tested approaches, and checked how well they predict the position of the peak in the spectral function corresponding to the IE energy.

A. GW +DMFT

1. Total energy

Fig. 2 show the total energy of several GW +DMFT methods and compares it to the results of LDA+DMFT, HF, GW and the exact solution. The LDA+DMFT results were already presented in our previous work [34], where we checked the accuracy of this approximation, and we showed the importance of using the exact double-counting within LDA+DMFT. The accuracy of the predicted total energy within LDA+DMFT is excellent, giving correct limit at large distance R of -2.0 Ry, and overall error below 1%, with only exception around the breking of the molecule ($R = 3.5 - 4$), where non-local corrections become important. At equilibrium distance, the error is less than 0.2%.

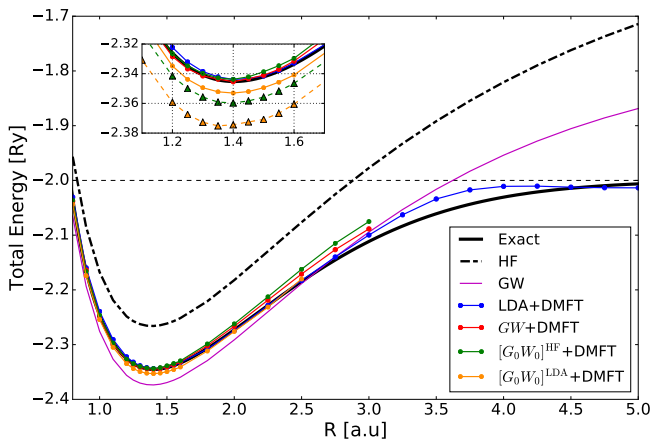


FIG. 2. (Color online) The ground state energy of $GW+DMFT$ versus R presented with the HF, GW, LDA+DMFT and exact result for comparison. (*inset*) We also added the total energy results of G_0W_0+DMFT without charge self-consistency (dashed lines).

As shown in Fig. 2 all methods tested here give better total energy than Hartree Fock (3.5% error) around the equilibrium distance ($R = 1.4$). The self-consistent GW gives error of approximately 1.3%. Inclusion of the correlations captured by the DMFT improves the total energy substantially, for example the fully self-consistent $GW+DMFT$ has an error of 0.3% (very similar to 0.2% in LDA+DMFT), In G_0W_0+DMFT calculation, with G_0 being based on the Hartree-Fock Hamiltonian ($[G_0W_0]^{HF}+DMFT$), the accuracy is almost as good as in $GW+DMFT$, while in $[G_0W_0]^{LDA}+DMFT$, the total energy is slightly less precise.

To show the effects of self-consistency of $GW+DMFT$ in detail, we display in the inset of Fig. 2 the G_0W_0+DMFT result at different self-consistent level. The dashed line shows G_0W_0+DMFT calculation where the total electronic charge is not updated, which is the common practice in solid state applications. In this approach, we first perform self-consistent LDA (or HF) calculation, and then we fix the Hartree potential V^H and GW self-energy $\Sigma^{GW} = G_0^{LDA(HF)}W_0^{LDA(HF)}$ at the LDA (HF) level, and we perform self-consistent DMFT calculation. Alternatively, when the electronic charge is updated self-consistently on the $GW+DMFT$ charge, the accuracy of the total energy clearly improves.

It is interesting to note that the charge self-consistency has much stronger effect on the total energy than the choice of the non-interacting G^0 in G^0W^0 . Both G^0W^0+DMFT methods are quite close to the $GW+DMFT$ results when the charge is updated, and much worse when charge is fixed at the LDA/HF level. Perhaps this is not very surprising, as the Hartree term contributes most to the total energy. For total energy calculation, the charge self-consistency is then much more important than the choice of G_0 , despite the fact that the G_0 based on LDA is substantially worse (37% error

for IE) than the HF spectra (2% error for IE).

In Fig. 2 we could not continue $GW+DMFT$ methods towards the atomic limit, most interesting correlated regime. The fully self-consistent $GW+DMFT$ and $G_0^{HF}W_0^{HF}+DMFT$ break down around $R = 3 a.u.$, while $G_0^{LDA}W_0^{LDA}+DMFT$ breaks down already at $R = 2.5 a.u.$. The reason for such dramatic failure of $GW+DMFT$ is the causality violation, which we will address in the next section. This is one of the most significant findings of our work, which shows that the self-consistent $GW+DMFT$ or G_0W_0+DMFT , when using exact double-counting, have no future in addressing the problem of strong correlations.

2. Causality breakdown

To solve the DMFT problem, and sum all local skeleton diagrams $\Phi_v[G_{loc}^R]$ we construct an auxiliary impurity problem, which has the same interaction v as the original problem, and $G_{loc}^R = \mathcal{G}_{imp}^R$. Note that in solid-state systems we need to renormalize interaction v due to screening effects, which is not needed here. Note also that this mapping of the local skeleton diagrams to an impurity model is exact, and no further approximation is made in this step. Furthermore, it is convenient to represent the impurity Green's function in terms of proper and improper self-energy (Σ_{imp} and Δ), i.e.,

$$\mathcal{G}_{imp} = \frac{1}{\omega - \varepsilon_{imp} - \Delta - \Sigma_{imp}} \quad (43)$$

where Σ is the self-energy due to the Coulomb interaction, while improper part Δ is due to the hybridization of this site with the medium, and is therefore commonly referred to as the Weiss mean field. The causality is violated if any of the three quantities \mathcal{G}_{imp} , Σ_{imp} , or Δ acquire positive imaginary part at any frequency point on the real or imaginary axis.

We want to write the DMFT self-consistency condition $\mathcal{G}_{imp} = \hat{P}G$ in such a way that the Weiss mean field Δ from Eq. 43 is expressed explicitly. To derive Δ , we will first eliminate the degrees of freedom which are not corrected by the DMFT (the 30 Gaussian orbitals Hilbert space, which has no overlap with the DMFT projectors). We will call this part of the Hilbert space r . The part of the Hilbert space, which is corrected by the DMFT will be denoted by d . In the second step, we will extract the Green's function of a single site, which is needed by the single site DMFT, and appears in the equation for hybridization Δ .

We start with the Green's function of $GW+DMFT$ from Eq.26:

$$G = \left(\omega + \mu - H^H - \Sigma^{GW} - \hat{E}(\Sigma_{imp} - \Sigma_{DC}^{GW}) \right)^{-1} \quad (44)$$

where we denoted $H^H = -\nabla^2 + v_{ext} + v^H$. We next write it in the block form, where dd part of the matrix is corrected by the DMFT, and the rest is not:

$$G = \begin{pmatrix} [\omega + \mu - H^H - \Sigma^{GW}]_{dd} - \Sigma_{imp} + \Sigma_{DC}^{GW} & -[H^H + \Sigma^{GW}]_{dr} \\ -[H^H + \Sigma^{GW}]_{rd} & [\omega + \mu - H^H - \Sigma^{GW}]_{rr} \end{pmatrix}^{-1} \quad (45)$$

We then eliminate the r part of the matrix, so that the G_{dd} becomes

$$G_{dd} = [\mathbb{1}(\omega + \mu - \Sigma_{imp} + \Sigma_{DC}^{GW}) - (H^H + \Sigma^{GW})_{dd} - M_{dr}M_{rr}^{-1}M_{rd}]^{-1} \quad (46)$$

where we denoted

$$\begin{aligned} M_{dr(rd)} &= [H^H + \Sigma^{GW}]_{dr(rd)} \\ M_{rr} &= [\omega + \mu - H^H - \Sigma^{GW}]_{rr}. \end{aligned} \quad (47)$$

We emphasized here that the dd part of G is still a matrix, in our case 2×2 for the two H atoms. In solid state, the dd part would be an infinite matrix, containing the correlated degrees of freedom, but written in real space. In the second step we express the Green's function of a

single site, as needed by the DMFT. We first define a matrix S :

$$S \equiv (H^H + \Sigma^{GW})_{dd} + M_{dr}M_{rr}^{-1}M_{rd} \quad (48)$$

so that

$$G_{dd} = [\mathbb{1}(\omega + \mu - \Sigma_{imp} + \Sigma_{DC}^{GW}) - S]^{-1} \quad (49)$$

and then the local Green's function becomes

$$G_{loc} = \frac{1}{\omega + \mu - \Sigma_{imp} + \Sigma_{DC}^{GW} - S_{11} - S_{12} \frac{1}{\omega + \mu - \Sigma_{imp} + \Sigma_{DC}^{GW} - S_{22}} S_{21}} \quad (50)$$

The crucial point is that in the correlated regime Σ_{imp} becomes large (diverges) and therefore we can neglect the last term in the denominator. Physically, this comes from the fact that in the correlated regime the correlated sites (H-atoms) decouple, and the effective hopping between them is thus cut-off by the appearance of large local Σ_{imp} , and therefore DMFT is able to recover the correct atomic limit. We thus have

$$G_{loc} = \frac{1}{\omega + \mu - \Sigma_{imp} + \Sigma_{DC}^{GW} - S_{11} - O(\frac{1}{\Sigma_{imp}})} \quad (51)$$

and comparing Eq. 51 with Eq. 43 reveals

$$\begin{aligned} \Delta &= \underbrace{(M_{dr} \frac{1}{(\omega + \mu)\mathbb{1}_R - H_{rr}^H - \Sigma_{rr}^{GW}} M_{rd})_{11}}_{\equiv \Delta_R} \\ &\quad + (\tilde{\Sigma}_{11}^{GW} - \tilde{\Sigma}_{DC}^{GW}) + O(\frac{1}{\Sigma_{imp}}) \end{aligned} \quad (52)$$

where the tilde notation on the self-energy means $\tilde{\Sigma}(\omega) = \Sigma(\omega) - \Sigma(\infty)$, and $\varepsilon_{imp} = -\mu + H_{dd}^H + \Sigma_{dd}^{GW}(\infty) - \Sigma_{DC}^{GW}(\infty)$. Note that $\Sigma_{11}^{GW} = \hat{P}\Sigma^{GW}$.

Although we used in Eq. 50 the fact that S is a 2×2 matrix, it is very easy to check that the resulting Eq. 52 is valid in general, even in the solid state with infinite number of correlated sites, a long as Σ_{imp} is large, and sites decouple.

While the first term in Eq. 52 (Δ_R) is always causal, the second term is generally not, and its imaginary part can have any sign. It has usually the non-causal sign, because the Σ_{DC}^{GW} tends to be larger than Σ_{dd}^{GW} . As we

will show in the section below, in the correlated regime Δ_R becomes small, and then the hybridization becomes non-causal.

Naively one would expect that Σ_{11}^{GW} and Σ_{DC}^{GW} would cancel, but they do not, because the projected local self-energy $\Sigma_{11}^{GW} = \hat{P}\Sigma^{GW}$ is

$$\Sigma_{11}^{GW} = [-GW]_{11} = -G_{loc}W_{1111} - \sum_{r \neq 1} G_{rr}W_{1r1r} \quad (53)$$

with the screened Coulomb interaction $W = v[1 - Pv]^{-1}$. Here $G_{11} = G_{loc}$. On the other hand, the double-counted term Σ_{DC}^{GW} is

$$\Sigma_{DC}^{GW} = -G_{loc}W_{loc}. \quad (54)$$

with the screened local interaction defined by $W_{loc} = v[1 - G_{loc}vG_{loc}]^{-1}$. The two terms are then always different.

Note also that within LDA+DMFT, this problem does not occur, because DC is static, and projected Kohn-Sham hamiltonian is also static, hence causality can not be violated.

In the dissociation regime ($R > 3.5 \sim 4.0$) the hopping between the two H-atoms should vanish, and this can be achieved by diverging impurity self-energy, so that the last term in the denominator of Eq. 50, vanishes. In this way we recover the exact atomic limit. And indeed this is how LDA+DMFT achieves the exact atomic limit. On the other hand GW +DMFT breaks down in this regime, and we will show below that this is because $\text{Im}\Sigma_{11}^{GW} < \text{Im}\Sigma_{DC}^{GW}$.

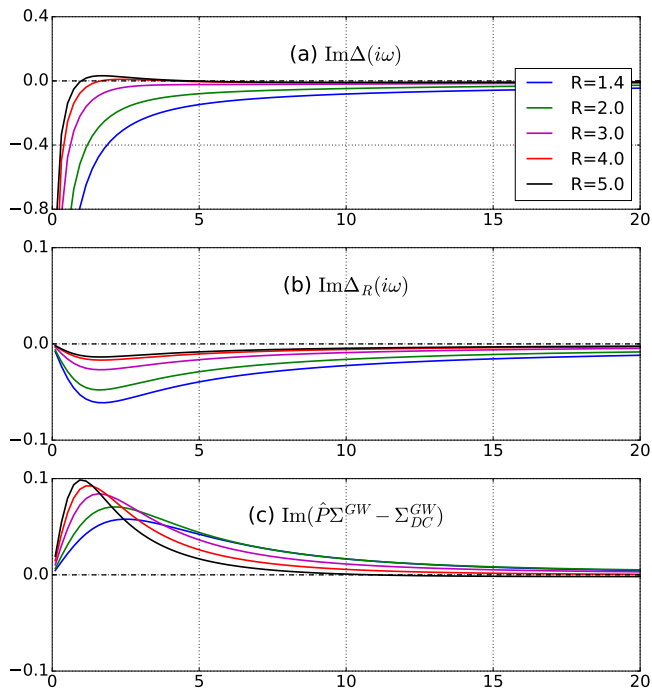


FIG. 3. (Color online) The imaginary part of (a) the hybridization function $\Delta(i\omega)$, and its component (b) $\Delta_R(i\omega)$ and (c) $\Delta\Sigma_{DC}^{GW}(i\omega)$ of Eq. (52). For the two cases ($R=4.0$ and 5.0) in which the causality break down, we took the result of the first iteration.

In Fig. 3(a) we show the imaginary part of Δ on the imaginary frequency axis. It is clear that for $R \gtrsim 3.5$ the imaginary part of Δ becomes positive in some frequency regime, violating the causality. In Figs. 3(b) and (c), we also present the terms appearing in Eq. 52, i.e., Δ_R and $(\hat{P}\tilde{\Sigma}^{GW} - \tilde{\Sigma}_{DC}^{GW})$. Clearly Δ_R is always causal, while $(\hat{P}\tilde{\Sigma}^{GW} - \tilde{\Sigma}_{DC}^{GW})$ has the wrong sign. In the weakly to moderately correlated regime, the last term in the denominator of (50) is large since the hopping between the two DMFT orbital, S_{12} , is substantial as the two site are close to each other. Therefore, this term outweighs the non-causal term $(\hat{P}\tilde{\Sigma}^{GW} - \tilde{\Sigma}_{DC}^{GW})$ and the causality is not yet violated in the weakly correlated regime.

One might ask then how is such causality violation avoided in the exact solution, i.e., when we replace Σ^{GW} with sum of all non-local Feynman diagrams. We know that in this case we should recover the exact solution. In this particular case, Σ_{DC} would vanish, as all terms are non-local and thus nothing is double-counted. We would then need to see that the projection of the non-local diagrams to the correlated site is positive. But there is a second possibility, which is more likely in low dimensional systems and molecules, namely that the non-local part of the self-energy diverges simultaneously with the local part, and therefore the separation into diverging local and well-behaved non-local part is not possible. In another words, we would not be able to neglect the last term in the denominator Eq. 50, because S_{12} is as large

as Σ_{imp} . In $GW+DMFT$, the GW self-energy is always Fermi-liquid like and it never diverges.

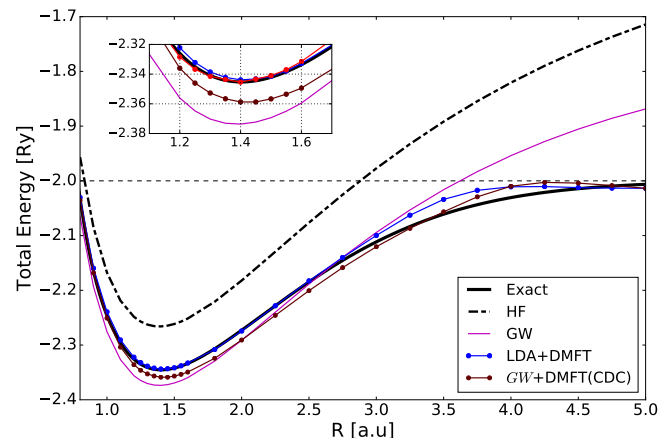


FIG. 4. The total energy result of $GW+DMFT$ with causal double-counting (CDC) scheme

As clear from the above argument, the causality is not violated if we take the CDC (Eq. (39)) because $P\Sigma^{GW} - \Sigma^{DC} = 0$. We present the total energy of this scheme in the Fig. 4.

In the moderate correlated regime (around $R = 1.4$), the CDC scheme is worse than exact double-counting scheme both in total energy and spectral function. The error of the total energy of $GW+DMFT$ with CDC, 0.8%, is worse than that of $LDA+DMFT$ (0.2%) or $GW+DMFT$ with exact DC (0.3%). However, it is very important that the CDC double-counting works correctly at the large distance regime, where all the exact double-counting schemes fail due to the causality violation. As clearly seen, the CDC total energy converges to -2.0.

Although CDC is an ad-hoc scheme, it allows $GW+DMFT$ to work in the strongly correlated regime without violating the causality. Since $GW+DMFT$ is meant for strongly correlated solids where Z is typically small, we argue that the $GW+DMFT$ for solid-state calculation is better when the CDC scheme is used and the effect of using the CDC instead of the exact double-counting should be investigated systematically.

3. Spectral function

In this section, we present the spectral function, the imaginary part of the Green's function summed over all diagonal component. We choose the zero of energy corresponding to dissociation of the molecule, so that the negative peak in spectra corresponds to the ionization energy. The Padé method is used for analytic continuation from imaginary frequency to real frequency. We mention in passing that Padé approximation is very accurate here, and we found only very minor sensitivity of the pole position (around 0.1%) depending on the choice of the input parameter for Padé method.

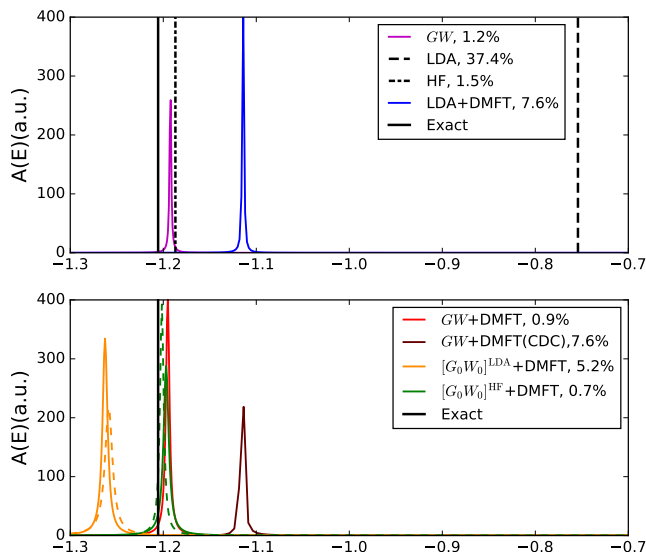


FIG. 5. (Color online) Spectral function for $R = 1.4$ where the exact IE is -1.206 a.u. Each errorbar is presented in the legend. (*upper panel*) GW , LDA , HF and $LDA+DMFT$ for comparison. (*lower panel*) $GW+DMFT$ schemes with different self-consistent conditions. The dashed lines indicates the result without charge self-consistency

In Fig. 5 we display the spectral function for $R = 1.4$ (the equilibrium distance), which corresponds to the moderately correlated regime. The peak position, measured from the vacuum (not from the chemical potential) corresponds to the IE. The LDA prediction for IE is 40% off the exact value. This failure is related to the band gap underestimation in solid-state calculation. On the contrary, the HF prediction is very good in this regime, and is only 1.5% off the exact value. The GW approximation slightly improves on HF , and its IE in the moderately correlated regime is only 1.2% of the exact value.

In Fig. 5a we also show the $LDA+DMFT$ prediction, which substantially improves the LDA value from 40% error down to 7.6% error. Nevertheless, the $LDA+DMFT$ spectra is not very accurate, as it builds on too inaccurate starting spectra.

We expect that GW in combination with $DMFT$ improves the GW result. Indeed when combining GW and $DMFT$ in a fully self-consistent way, the error is only 0.9% and when using G_0W_0 from HF (which itself is quite precise), the error is only 0.7%. Somewhat worse is the result of G_0W_0+DMFT when G_0 is taken from LDA . The error in this case is quite comparable to $LDA+DMFT$ error, but it seems the combination of $DMFT$ and G_0W_0 overcorrects the LDA .

Notice also that the charge self-consistency has almost no effect on the spectra, while we showed before that charge self-consistency is crucial for the accuracy of the total energy. On the other hand, the choice of G_0 is crucial for spectra, but not for the total energy.

We note that the $GW+DMFT$ with CDC is worse than . We attribute this inaccuracy to the fact that the CDC scheme includes the interactions between the $DMFT$ space and the rest of Hilbert space, which is not supposed to be involved in the local impurity self-energy. Therefore, CDC scheme in this scheme is less precise than the $GW+DMFT$ with the exact DC .

On the other hand, at the large separation limit (Fig. 6) where the correlation effects are strong, the CDC scheme is the only $GW+DMFT$ method that works without causality violation. It successfully reproduces the spectral function close to the exact value and its quality is comparable to that of $LDA+DMFT$. All other methods without the $DMFT$ treatment, LDA , HF and GW , are far from the exact ones due to the failure of perturbation theory.

We notice that $DMFT$ considerably improves the total energy of GW in this regime, while the spectra seems barely affected. This is because the renormalization amplitude from local GW self-energy and the $DMFT$ self-energy are almost the same in this weakly correlated regime, and their values are 0.935 and 0.928, respectively.

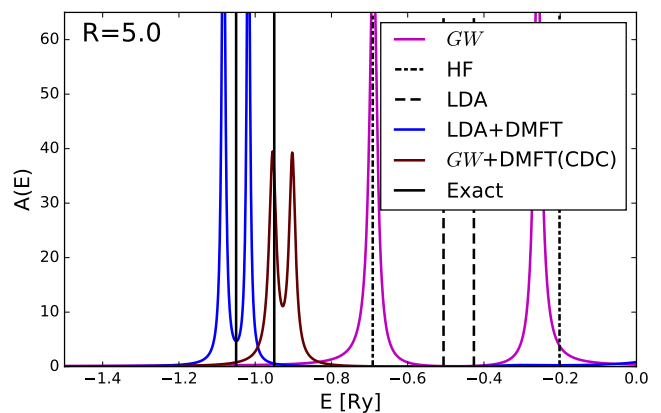


FIG. 6. The spectral function (*upper panel* $R=1.4$, *upper panel* $R=5.0$) calculated by $GW+DMFT$ with causal double-counting (CDC) scheme

B. QSGW+DMFT

As shown above, the self-consistent $GW+DMFT$ fails in the correlated regime due to causality violation, which comes from the fact that double-counted self-energy is dynamic and too large. In $QSGW$ the GW spectra is represented by an approximate static Hermitian Hamiltonian, and in this case we expect that approximating the double-counting by a static value might be a reasonable choice. We denoted this choice by SDC . As discussed above, the static DC term tends to over-count the renormalization effects, and this can be somewhat remedied by choosing dynamic double counting, which we denote by DDC .

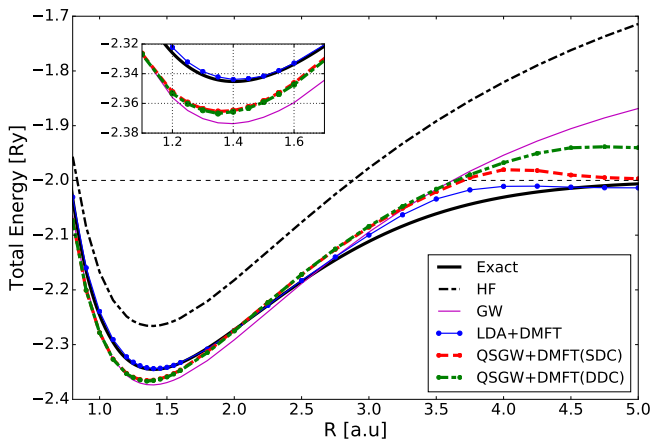


FIG. 7. (Color online) The ground state energy of the QSGW+DMFT results with two different schemes of double-counting. The inset shows the magnification around the equilibrium distance.

In Figs. 7 we display the total energy of QSGW+DMFT together with GW, LDA+DMFT and exact total energy. Because the quasiparticle approximation is not derivable from a functional, the energies are unfortunately not very good. At equilibrium, the QSGW+DMFT energy is very similar to GW energy, while in the correlated regime the addition of DMFT slightly improves the GW energy. Nevertheless, the dynamic double-counting does not recover correct atomic limit, even though DMFT is expected to be exact in the atomic limit. This failure is again due to the double-counting issue, namely, when impurity self-energy is diverging, the hybridization should vanish, but when a dynamic double-counting is used, hybridization does not vanish, and the atomic limit is not reached. In solid state applications, this would correspond to a missed Mott transition in the strongly correlated limit. We see in Fig. 7 that only a static DC correctly reproduces atomic limit. But unfortunately the total energy is substantially worse than corresponding LDA+DMFT result. This is not unexpected, as only methods derivable from a functional are expected to give precise total energies. [43]

Next we show the spectral functions of QSGW+DMFT at equilibrium position. Fig. 8 compares the GW, LDA+DMFT and two version of QSGW+DMFT schemes with the exact solution. For the static double-counting (SDC) scheme, the spectra is not good, and very comparable to LDA+DMFT result. The origin of the error is however quite different, in QSGW it is due to the double renormalization by both the GW and DMFT, while in LDA+DMFT it is due to missing non-local correlations.

The dynamic double-counting scheme (DDC) substantially improves the spectra in this weakly correlated regime, and the error of IE is only 1%, comparable to the fully self consistent GW+DMFT. However, the DDC

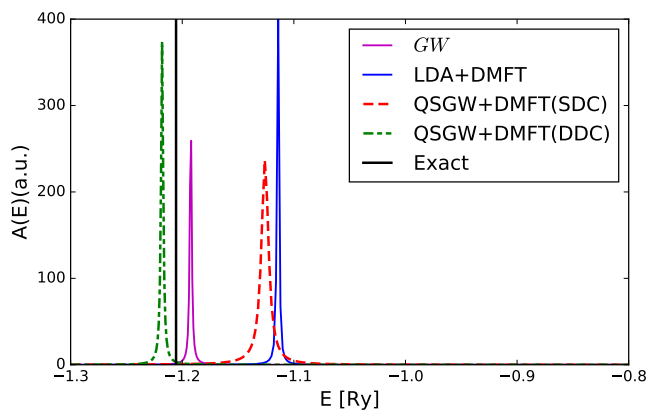


FIG. 8. (Color online) The QSGW+DMFT spectral results with two different double-counting schemes at $R = 1.4$, compared with GW, LDA, HF and LDA+DMFT

scheme is much worse in the strongly correlated regime, both for energy and for spectra.

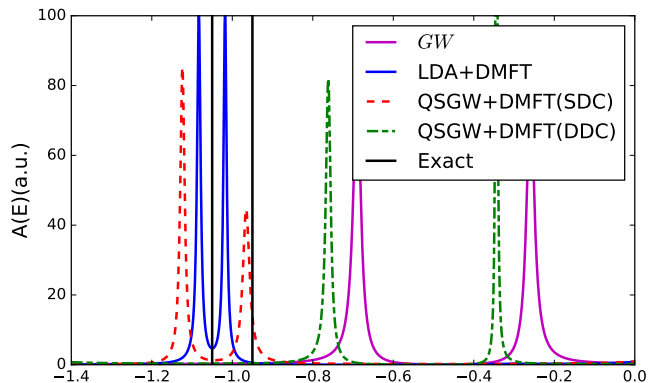


FIG. 9. (Color online) Spectral function for $R = 5.0$. (*upper panel*) Perturbative schemes: HF, LDA and GW. (*lower panel*) LDA+DMFT and QSGW+DMFT with two different double-counting functional.

In Figs. 9 we present results at $R = 5.0$, deep in the correlated regime, where excitations of two almost independent H atoms are expected, with the value close to -1.0 Ry. In this regime QSGW+DMFT with static double-counting (SDC) and LDA+DMFT perform reasonably well, while dynamic double-counting (DDC) fails very similarly to GW approximation. This failure of DDC was also reported in Ref. [27], where a similar scheme to our DDC was tested on SrVO_3 .

IV. SUMMARY

We have implemented GW+DMFT and QSGW+DMFT scheme for H_2 molecule, and we compared the total energy and spectral function with the

exact result, and LDA+DMFT. For GW +DMFT, five different calculations have been performed: (i) fully self-consistent GW +DMFT, (ii) $[G_0W_0]^{\text{HF}}$ +DMFT where G_0 is taken from Hartree-Fock, (iii) $[G_0W_0]^{\text{LDA}}$ +DMFT with G_0 from LDA, (iv) $[G_0W_0]^{\text{HF}}$ +DMFT but without charge self-consistency, (v) $[G_0W_0]^{\text{LDA}}$ +DMFT without charge self-consistency.

1) In the strongly correlated regime only LDA+DMFT and QSGW+DMFT with static double-counting give good spectra, and only LDA+DMFT gives good total energy.

2) Most of GW +DMFT schemes fail in the correlated regime due to causality violation. While QSGW+DMFT does not suffer causality violation, it performs reasonably well in the correlated regime only when using the static double-counting.

3) In the Fermi liquid regime of weak to moderate correlations, fully self-consistent GW +DMFT is excellent, both for total energy and spectra.

4) The spectra in the weakly correlated regime is also very accurately obtained by $[G_0W_0]^{\text{HF}}$ +DMFT, but less precise with $[G_0W_0]^{\text{LDA}}$ +DMFT. The QSGW+DMFT with static double-counting, which performs well in correlated regime, is less precise here, as it renormalizes spectra twice. The dynamic double-counting remedies this

shortcoming in the weakly correlated regime, but fails in the strongly correlated regime.

5) Total energy in the weakly correlated regime is good in all GW +DMFT schemes (but not in QSGW+DMFT), provided the charge is computed self-consistently.

In summary, the strongly correlated regime is more challenging to describe by GW +DMFT as previously thought, and the causality violation seriously impacts the prospects of using GW +DMFT in this regime. On the other hand, using QSGW+DMFT in this regime leads to somewhat better spectra than employing less demanding LDA+DMFT, but it does not lead to better total energies.

V. ACKNOWLEDGMENTS

J.L. thanks Lorenzo Sponza for discussion of the causality issue. J.L. was supported by the Rutgers Physics Departmental Fellowship and NSF-DMR 1405303. K.H. was supported by the NSF-DMR 1405303 and the Simons foundation under project ‘‘Many Electron Problem’’.

-
- [1] P. Hohenberg and W. Kohn, *Phys. Rev.* **136**, B864 (1964).
- [2] W. Kohn and L. J. Sham, *Phys. Rev.* **140**, A1133 (1965).
- [3] A. Georges and G. Kotliar, *Phys. Rev. B* **45**, 6479 (1992).
- [4] A. Georges, G. Kotliar, W. Krauth, and M. J. Rozenberg, *Rev. Mod. Phys.* **68**, 13 (1996).
- [5] Q. Si and J. L. Smith, *Phys. Rev. Lett.* **77**, 3391 (1996).
- [6] H. Kajuter, Pd.D. Thesis, Rutgers University (1996).
- [7] R. Chitra and G. Kotliar, *Phys. Rev. Lett.* **84**, 3678 (2000).
- [8] T. Maier, M. Jarrell, T. Pruschke, and M. H. Hettler, *Rev. Mod. Phys.* **77**, 1027 (2005).
- [9] G. Kotliar, S. Y. Savrasov, K. Haule, V. S. Oudovenko, O. Parcollet, and C. A. Marianetti, *Rev. Mod. Phys.* **78**, 865 (2006).
- [10] B. Amadon, S. Biermann, A. Georges, and F. Aryasetiawan, *Phys. Rev. Lett.* **96**, 066402 (2006).
- [11] K. Haule and T. Birol, *Phys. Rev. Lett.* **115**, 256402 (2015).
- [12] N. Lin, C. A. Marianetti, A. J. Millis, and D. R. Reichman, *Physical Review Letters* **106**, 096402 (2011).
- [13] C. Weber, D. J. Cole, D. D. ORegan, and M. C. Payne, *Proceedings of the National Academy of Sciences* **111**, 5790 (2014).
- [14] L. Hedin, *Phys. Rev.* **139**, A796 (1965).
- [15] G. Onida, L. Reining, and A. Rubio, *Rev. Mod. Phys.* **74**, 601 (2002).
- [16] P. Sun and G. Kotliar, *Phys. Rev. B* **66**, 085120 (2002).
- [17] S. Biermann, F. Aryasetiawan, and A. Georges, *Phys. Rev. Lett.* **90**, 086402 (2003).
- [18] J. M. Tomczak, M. van Schilfhaarde, and G. Kotliar, *Phys. Rev. Lett.* **109**, 237010 (2012).
- [19] T. Miyake, C. Martins, R. Sakuma, and F. Aryasetiawan, *Phys. Rev. B* **87**, 115110 (2013).
- [20] V. Brouet, P.-H. Lin, Y. Texier, J. Bobroff, A. Taleb-Ibrahimi, P. Le Fèvre, F. Bertran, M. Casula, P. Werner, S. Biermann, F. Rullier-Albenque, A. Forget, and D. Colson, *Phys. Rev. Lett.* **110**, 167002 (2013).
- [21] M. S. Hybertsen and S. G. Louie, *Phys. Rev. B* **34**, 5390 (1986).
- [22] F. Aryasetiawan and O. Gunnarsson, *Reports on Progress in Physics* **61**, 237 (1998).
- [23] S. V. Faleev, M. van Schilfhaarde, and T. Kotani, *Phys. Rev. Lett.* **93**, 126406 (2004).
- [24] M. van Schilfhaarde, T. Kotani, and S. Faleev, *Phys. Rev. Lett.* **96**, 226402 (2006).
- [25] T. Kotani, M. van Schilfhaarde, and S. V. Faleev, *Phys. Rev. B* **76**, 165106 (2007).
- [26] J. M. Tomczak, M. Casula, T. Miyake, F. Aryasetiawan, and S. Biermann, *EPL (Europhysics Letters)* **100**, 67001 (2012).
- [27] R. Sakuma, P. Werner, and F. Aryasetiawan, *Phys. Rev. B* **88**, 235110 (2013).
- [28] C. Taranto, M. Kaltak, N. Parragh, G. Sangiovanni, G. Kresse, A. Toschi, and K. Held, *Phys. Rev. B* **88**, 165119 (2013).
- [29] J. M. Tomczak, M. Casula, T. Miyake, and S. Biermann, *Phys. Rev. B* **90**, 165138 (2014).
- [30] S. Choi, A. Kutepov, K. Haule, M. van Schilfhaarde, and G. Kotliar, *Npj Quantum Materials* **1**, 16001 EP (2016).
- [31] T. Ayrál, P. Werner, and S. Biermann, *Phys. Rev. Lett.* **109**, 226401 (2012).
- [32] P. Hansmann, T. Ayrál, L. Vaugier, P. Werner, and S. Biermann, *Phys. Rev. Lett.* **110**, 166401 (2013).

- [33] T. Ayrál, S. Biermann, and P. Werner, *Phys. Rev. B* **87**, 125149 (2013).
- [34] J. Lee and K. Haule, *Phys. Rev. B* **91**, 155144 (2015).
- [35] G. Baym and L. P. Kadanoff, *Phys. Rev.* **124**, 287 (1961).
- [36] G. Baym, *Phys. Rev.* **127**, 1391 (1962).
- [37] M. Boninsegni, N. V. Prokof'ev, and B. V. Svistunov, *Phys. Rev. E* **74**, 036701 (2006).
- [38] S. H. Vosko, L. Wilk, and M. Nusair, *Canadian Journal of Physics* **58**, 1200 (1980).
- [39] K. Haule, *Phys. Rev. Lett.* **115**, 196403 (2015).
- [40] J. M. Tomczak, *Journal of Physics: Conference Series* **592**, 012055 (2015).
- [41] G. Hadinger, M. Aubert-Frecon, and G. Hadinger, *J. Phys. B: At., Mol. Opt. Phys.* **22**, 697 (1989).
- [42] T. H. Dunning, *The Journal of Chemical Physics* **90** (1989).
- [43] A. Stan, N. E. Dahlen, and R. van Leeuwen, *EPL (Europhysics Letters)* **76**, 298 (2006).